ILASS 2008
Sep. 8-10, 2008, Como Lake, Italy

Paper ID ILASS08-6-4

DISPERSED FLOW OF FUEL DROPLETS IN THE INTAKE VALVE REGION OF A PORT-INJECTED ENGINE

Begg, S.*, Hindle, M.°, Mason, D.* and Heikal, M.*

* Sir Harry Ricardo Laboratories, Internal Combustion Engine Group, School of Environment and Technology, University of Brighton, Brighton, BN2 4GJ, UK.
°Formerly ICEG, University of Brighton, UK.

ABSTRACT

A phenomenological study of the characteristics of gasoline fuel droplets, dispersed in the gas phase in the exit region downstream of the intake valves a modified production BMW Valvetronic cylinder head is presented. A steady-state flow rig was used to simulate the intake conditions and fuel injection in a port-injected engine, with optical access to the intake port and pent-roof combustion chamber. The intake valve lift was varied manually over the range of 0.34mm to 9mm. Several experimental techniques (including photography, imaging, LDA, PIV and PDA) were to measure the characteristics of the intake port discharge coefficient, mean and turbulent airflow and the liquid fuel spray over a range of peak intake valve lifts and flow conditions. Two transitional phases in the airflow and fuel spray delivery were identified; namely for valve lifts greater than 3 mm and those less than 1 mm. The classical forward tumble air motion observed at full valve lift was replaced by twin, weakly rotating reverse tumble structures at the lowest lifts located either side of a high-speed exit jet. The distribution of the air and droplet axial and radial velocity components close to the high speed jet was bi-modal and the droplet mean diameter was reduced by an order.

1. INTRODUCTION

Modern gasoline engines use variable valve technology to enhance torque and reduce fuel consumption and CO_2 emissions through an improvement in the part-load, four-stroke cycle efficiency. The simplest strategy involves phasing of the timing of the camshaft that operates the intake valves [1, 2] or additionally, the exhaust valves. The approach used by BMW, in their Valvetronic engine, uses an advanced mechanical system that provides continuously variable valve lift (CVVL) for throttle-less engine load control. The timing of the opening of the intake and exhaust valves can be controlled independently; however the duration of the valve opening is dependent upon the height of the valve lift. A part load reduction in pumping losses can be achieved as the intake of air and fuel is metered by a low valve lift event. Fuel consumption improvements of up to 20% at idle engine operating conditions have been reported for stoichiometric operation [3-4]. Under these conditions the peak valve lift can be less than 0.5 mm.

The mixture preparation processes in a gasoline engine are enhanced by high flow velocities in the valve gap region. These velocities are reduced when the engine is run at low speeds and when a throttle valve is used to control engine load. CVVL engines use low valve lifts, instead of throttling, to increase the flow velocities in the valve gap region and improve mixture preparation [9, 10]. At the engine idle condition, the lowest valve lift occurs and the flow of the mixture of gas and fuel through the valve gap and within the combustion chamber is significantly altered [11-12]. The primary large scale rotating structures are no longer observed [11, 15]. So-called ‘secondary droplet break-up’ (aerodynamic break-up due to shear forces resulting from the relative velocity exceeding the liquid surface tension force) has not been observed [9]. However, a significant reduction in fuel droplet size was measured downstream of the valve orifice area for a valve lift of 1mm. Additionally, the volume of fuel that is present in the orifice area affects the intake gas flow into the chamber and can lead to fuel pooling, wall film stripping and gravitational effects [16, 17]. The characteristics of a droplet in such a system involving numerous individual droplets can only be described by the average behaviour of droplets in a given region.

A series of experiments were devised to investigate the effects of varying the intake valve lift upon the steady flow and the fuel spray characteristics in the intake port and region downstream of the intake valve curtain. A modified BMW Valvetronic cylinder head was used.

In the first section, the experimental approach and apparatus are briefly outlined. In the second section, a selection of results are presented and discussed. In the final section, the conclusions of the experimental study are summarised.

2. EXPERIMENTAL APPROACH

Experimental measurements of a port-injected gasoline fuel spray, gas flow dynamics and port discharge coefficient were examined in a steady-state flow rig over a range of intake valve lifts. The in-cylinder gas flow velocity components were measured using Particle Image Velocimetry (PIV) and 2-component, coincident Laser Doppler Anemometry (LDA) in the absence of fuel injection. The characteristics of the fuel spray and droplets (diameter and velocity components) were measured using a Phase Doppler Anemometer. The droplet velocity and sizes were measured independently. High-speed

photography and high resolution, laser light illuminated, imaging were used additionally to investigate the large scale structures in the fuel spray.

Table 1: Specification of engine and fuel system

Cylinder head	BMW N42B20
Chamber geometry	Pent-roof
Number of valves	2 intake, 2 exhaust
Valve lift range	0.34 to 9 mm
Fuel injection	4-hole PFI
Injection pressure	3.5 bar
Fuel temperature	22 °C
Fuel type	Iso-octane (2, 2, 4 TMP)
Injection frequency	1 Hz

2.1 Apparatus

2.1.1 Steady-state flow rig

The steady-state flow rig was installed in a test cell at the Sir Harry Ricardo Laboratories at the University of Brighton. The fuel injection system, air box, variable geometry intake manifold and cylinder head of a production BMW Valvetronic engine (type N42B20) were used for the study. The specification of the engine and fuel injection system is given in Table 1.

Compressed dry air was pumped through the test rig via a damping volume. The mass flow of air was metered by a critical flow nozzle (type Toroidal Venturi, ISO9300). The experimental rig was instrumented with 0-10 bar and 0-2 bar pressure transducers (type Druck PDCR 800) with an error of 0.01 bar and 1 mbar ± 1.5% full-scale deflection respectively. Temperature was measured using thermocouples (K-type) to an accuracy of ± 0.7°C.

The cylinder head and one intake port were modified to allow optical access to the intake port (from the base and side) and the valve gap region within the pent-roof chamber. The flow discharged into a Perspex rectangular box section. This permitted more accurate measurements and improved flow visualisation close to the valve exit without the periodic fluctuations associated with reciprocating motion of the piston that would be found in an engine. The experimental assembly is shown in Fig. 1. The intake valve lift was varied using individual micrometer adjusters fitted to each valve stem with an accuracy of ± 0.005 mm.

The fuel injection equipment comprised standard automotive components. A Siemens Deka port fuel injector was operated at an injection pressure of 3.5 bar. The temporal and spatial distribution of the fuel droplet velocities and diameters in the spray were previously studied by the authors using PDA in a tall spray chamber under atmospheric and quiescent conditions [18]. High-speed photography was used to confirm the point of impingement of the fuel spray on the back of the intake valve (cone and jet separation angles) and to compare the symmetry in the rate of penetration between each pair of jets directed in each port. From this quiescent study [18] instantaneous peak velocities were recorded in excess of 25m/s close to the nozzle, where mean droplet diameters were of the order of 15 to 20µm. At a distance equivalent to nozzle valve separation average droplet sizes were in the range of 40 to 60µm in diameter, with an average velocity in the region of 16 to 18m/s. Data validation rates were generally greater than 70%. These results were used as a starting point for subsequent investigations.

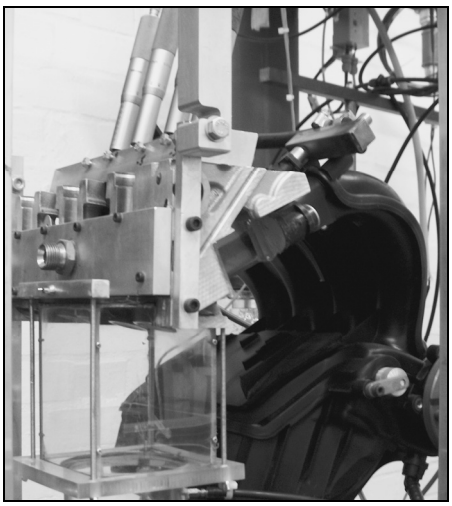

Figure 1: Modified cylinder head and steady-state flow rig assembly

2.2 Brief description of applied optical techniques

The optimisation of each of the techniques formed an important part of the investigation. However, a full description of the optical techniques is beyond the scope of this paper and therefore a brief summary is given below. In all cases, the mid-cylinder, mid-valve and near-wall, tumble (TP) and cross-tumble (CT) planes were studied as shown in Fig. 2.

The in-cylinder steady flow air motion was measured using a LaVision PIV system. Corn oil droplets, with a mean diameter of 1-2 µm were used to seed the gas flow. Fifty image pairs with a resolution of 1376x1040 pixels were acquired for each condition and analysed using the cross-correlation technique with a grid spacing of 32x32 pixels and a 50% window overlap. An average and RMS image were computed.

The instantaneous in-cylinder gas velocity components were measured at individual point locations using a forward scatter, coincident mode, Dantec 85 mm probe LDA. Again, corn oil was used to seed the flow. A programmable traverse was used to move the transmission optic and collection optics over a 5 mm x 5 mm grid in tumble plane TP2. The positional error was ± 0.1 mm. 10,000 validated measurements were acquired at each location. The test conditions were then repeated with fuel injection. High-speed ciné (Phantom V7.1 camera) and Laser Light Scattering Imaging were applied in a sheet through the port and cylinder planes. These images (in conjunction with the LDA and PIV results) were used to define a series of locations for the PDA measurements.

The fuel droplet size and velocity distributions were measured close to the valve exit using a forward scatter PDA. The BSA P70 PDA processor was triggered with the start of injection (SOI) pulse. Non-coincident data was collected for either 10,000 measurements or 60 s duration (in the axial velocity direction, (u)) and 5,000 measurements or 60 s duration (in the radial velocity direction, (v)). The final parameters of the optimised PDA configuration are shown in Table 2. The estimated standard error in the diameter measurements was of the order of ± 2 micron

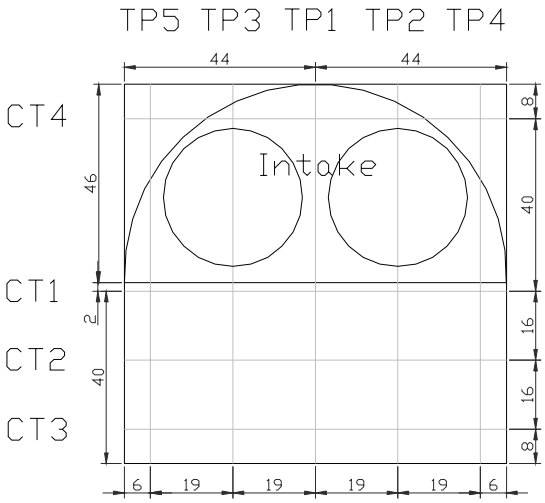

Figure 2: Location of the measurement planes

2.3 Test conditions

The experimental flow rate conditions for the test rig were derived from the engine data shown in Fig. 3 and were selected to be representative of varying engine speed and load conditions on the EUDC drive cycle. The coloured bands show how the peak intake valve lift varies with engine operation. The tests were conducted with the variable geometry manifold in the extended (long) position. For the cases presented in this paper, a fixed pressure drop condition of 40 mbar across the intake valve was used or a fixed mass flow rate of 0.01 kgs^{-1}. At full valve lift conditions, the mass flow rate of air was approximately 0.07 kgs^{-1} at the 40 mbar condition. The injection duration was 2-3 ms, corresponding to an injected fuel mass of approximately 4-5 mg. The optimal injection frequency for the steady state rig was 2 Hz.

Table 2: Optimised PDA configuration

PDA Parameters		Classical PDA	
Wavelength	(nm)	514.5	488
Focal length	(mm)	310	310
Probe volume diameter	(μm)	47	44
Probe volume length	(mm)	1.044	0.990
Beam half-angle	(º)	2.56	2.56
Fringe spacing	(μm)	5.76	5.46
No. of fringes	(-)	8	8
Beam diameter	(mm)	2.2	
Expander ratio	(-)	1.98	
Sphericity Validation	(%)	10	
Scattering Angle	(°)	77.5	

2.4 The intake port discharge coefficient

The discharge coefficient was used to determine the efficiency of the induction system (port and valve) over the range of valve lifts. The discharge coefficient (C_d) is a measure of the hydraulic resistance to a flow. It is the ratio of air mass flow rates defined in Equation (1):

$$C_d = \frac{\dot{m}_{ac}}{\dot{m}_{th}} \qquad \text{Eq(1)}$$

where $\dot{m}_{ac}$ is the mass flow rate as measured at a venturi nozzle and $\dot{m}_{th}$ is the theoretical mass flow rate. The actual mass flow rate (venturi) $\dot{m}_{ac}$ is given by:

$$\dot{m}_{ac} = k_{vent} \frac{p_{vent}}{\sqrt{T_{vent}}} \qquad \text{Eq(2)}$$

where p_{vent} is the absolute pressure measured at the venturi throat, T_{vent} is the air temperature at the venturi throat and k_{vent} is the nozzle number specific to the venturi measurement device. The theoretical mass flow rate $\dot{m}_{th}$ is given by Equation 3:

$$\dot{m}_{th} = A\left(\sqrt{2\rho_{cyl}\Delta p}\right) \qquad \text{Eq(3)}$$

where ρ_{cyl} is the air density in the cylinder which is assumed equal to that at the intake valve orifice, Δp is the pressure difference across the intake valve and A is an area representative of the flow restriction (intake valve gap). In this case, a minimum geometric flow area was determined for a range of valve lifts using the criteria in [19].

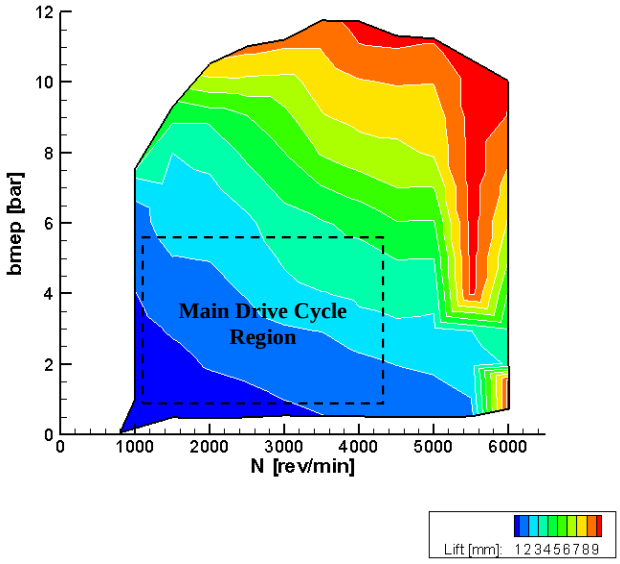

Figure 3: Variation in peak intake valve lift with engine speed and load for the BMW Valvetronic engine.

The discharge coefficient of the steady flow rig was measured over a range of valve lifts at the 40mbar fixed pressure test condition. The variation in discharge coefficient is shown in Fig. 4 below.

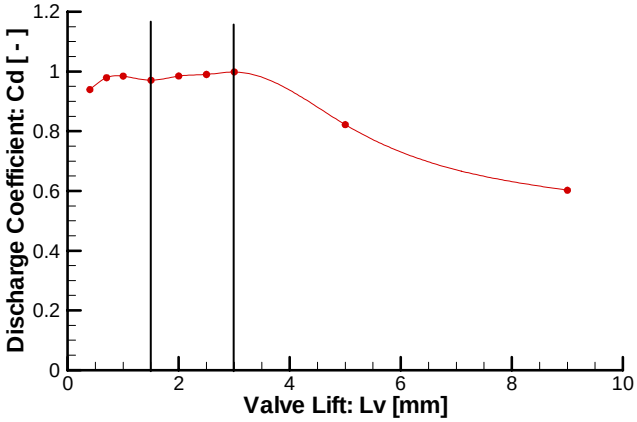

Figure 4: Variation in discharge coefficient with valve lift for a fixed pressure drop of 40 mbar.

In the range of 0.34<L_v<3, the discharge coefficient was close to unity, indicative of an attached flow regime, with some partial detachment for valve lifts less than 1.5 mm. For lifts greater than 3 mm, separation at the sharp edges of the valve led to a flow contraction. At the maximum valve lift, a free flow regime existed and C_d was independent of Reynolds number.

3. RESULTS AND DISCUSSION

3.1 In-cylinder mean air motion

The in-cylinder mean flow structures observed over the translational range of peak valve lifts from 0.4 mm to 3 mm are presented in Fig. 5 for the fixed pressure drop condition of 40 mbar, in tumble plane TP2. It should be noted that the colour scales have been adjusted as the magnitude of the in-cylinder velocity increases with increasing valve lift.

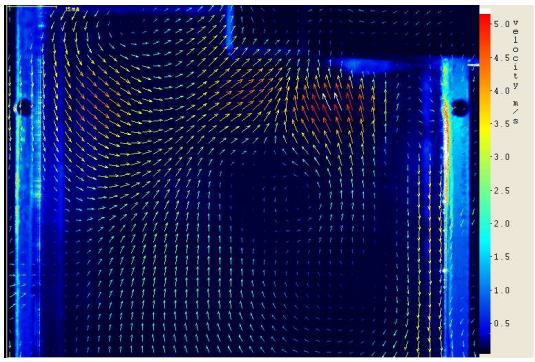

L_v = 0.4 mm

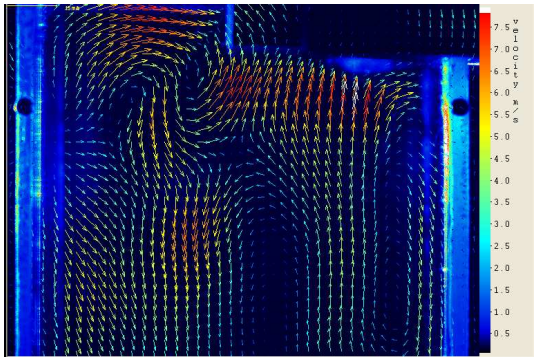

L_v = 1.5 mm

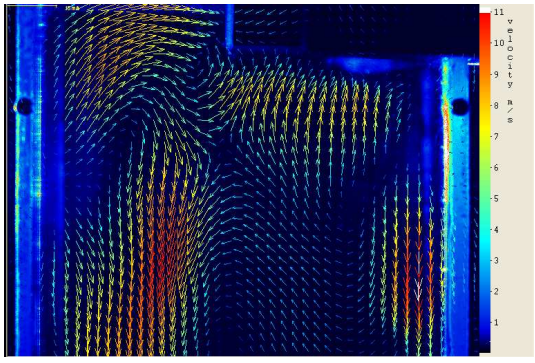

L_v = 2.5 mm

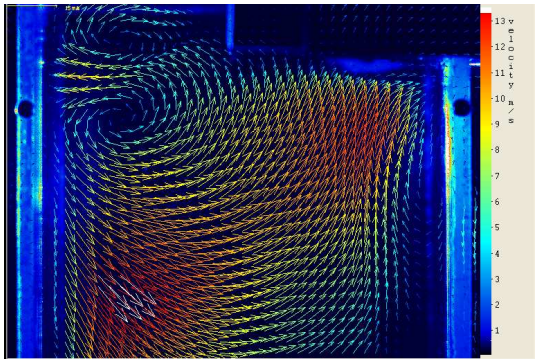

L_v = 3.0 mm

Figure 5: Mean air motion in tumble plane, TP2

For valve lifts greater than 3 mm, the classical forward tumble motion was dominant within the cylinder. A second counter-rotating vortex-like structure was observed to form above the intake jet. In the range of L_v=1.5-2.5 mm, the forward tumble motion was seen to breakdown into a disorganised flow. For valve lifts below this value, the dominant flow occurred on the intake side of the chamber, establishing a reverse tumble motion. As the valve lift was decreased, the flow exited the valve area in all directions equally and the cross-tumble velocity component became more significant. An example of the cross-tumble flow patterns is shown in Fig. 6 for cross-tumble plane CT1. The flow is asymmetric in the cross-tumble plane which was apparent at all valve lifts and was attributed to the curvature of the intake manifold that induced a cork-screwing effect upon the flow.

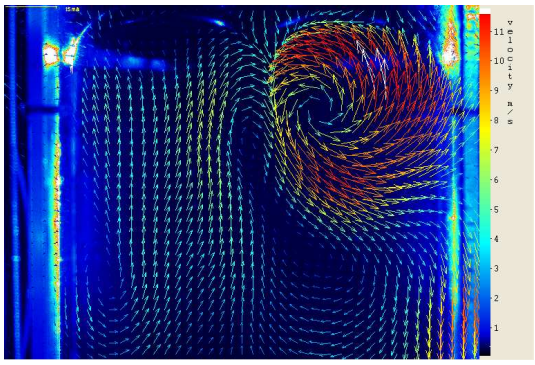

Figure 6: Mean air motion in cross-tumble plane, CT1 for L_v = 2.5 mm, fixed pressure drop of 40 mbar

3.2 Point velocity measurements

The instantaneous velocity was measured over a grid of points in the region of the valve exit jet for a range of valve lifts. A comparison in the mean steady flow characteristics and turbulence intensity with valve lift in the exit jet and upper cylinder regions is shown in Figs. 7 and 8 for L_v = 0.4mm and L_v = 9mm respectively and for a mass flow rate of 0.01kg/s. In the high lift case, the LDA measurements showed a good agreement with the PIV data. In the low lift case, a high velocity, narrow exit jet was measured at the top of the cylinder. The validated data rate within the jet was approximately 1.4 kHz. The estimated thickness of the exit jet (based upon data rate) was approximately 2 mm. The high velocity air flow continued across the top of the cylinder and down the exhaust-side wall and corresponded to the region of

minimum turbulence intensity. Peak turbulence intensity was approximately 600%.

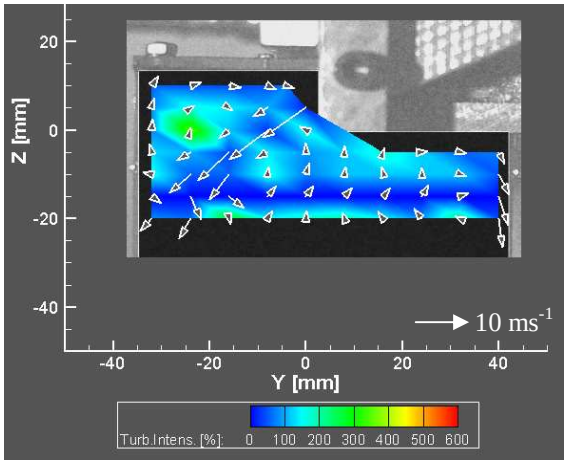

Figure 7: Mean steady flow and turbulence intensity for L_v= 9 mm, fixed air mass flow rate of 0.01 kgs^{-1} in TP2

In comparison to the 0.4mm case, the magnitude of the mean velocity of the exit jet at a valve lift of 9mm was approximately one quarter of that observed at the lowest lift. The turbulence intensity was one third of that observed at a valve lift of 0.4mm.

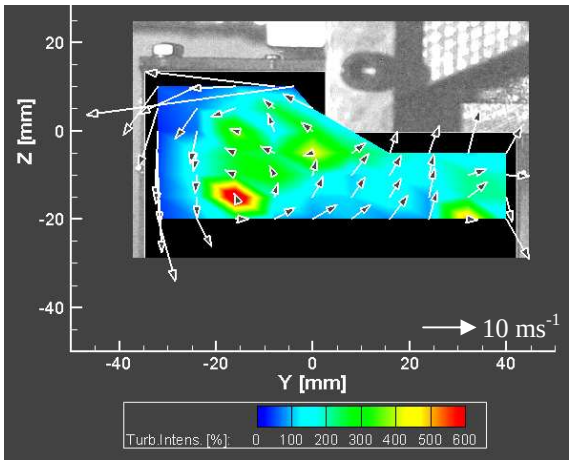

Figure 8: Mean steady flow and turbulence intensity for L_v= 0.4 mm, fixed air mass flow rate of 0.01 kgs^{-1} in TP2

The velocity distribution of measurements of both the axial and radial velocity components at the low lift case is shown in Fig. 9a, b for a location in the high speed jet. There was a broad spread in both velocity components. The form approximated to a Gaussian distribution. The radial velocities measured were negative (towards the exhaust side) whereas the axial component was distributed about a mean of approximately -8 ms^{-1}. In this region, the axial fluctuation due to flow induced instabilities was the greatest observed.

3.3 In-cylinder fuel distribution

The characteristics of the fuel injection process were captured using laser-light sheet illuminated imaging. A comparison of the results is presented in Fig. 10a, b, c for three valve lift ranges; 0.4 to 1 mm, 1 to 3 mm and 3 to 9 mm. Tumble plane 2 showed the highest concentration of fuel.

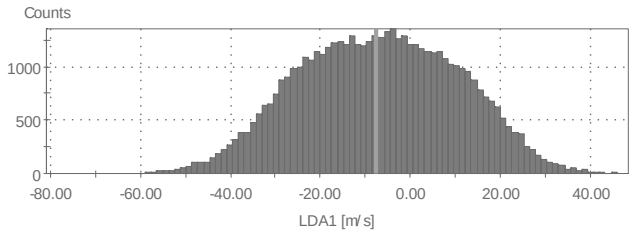

(a) Axial Velocity Component

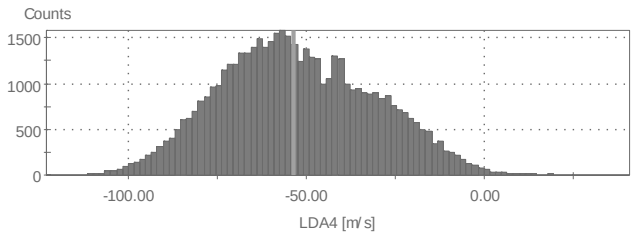

(b) Radial Velocity Component

Figure 9: Velocity histograms at 10 mm below the gas face for L_v= 0.4 mm and for an air mass flow rate of 0.01 kgs^{-1}

At high valve lifts the jet flow was predominantly over the valve toward the exhaust-side wall. In the case of high valve lift and low valve orifice velocity (low mass flow rate), gravitational break-up from the intake valve surface was observed. In addition, a large proportion of the fuel exited the intake valve on the intake-side region due to a reduction in the angular momentum of the tumble bulk flow pattern. At intermediate valve lifts, the jet flow was evenly distributed around the valve periphery. Discrete droplets were observed. At low valve lifts, an initial jet was observed followed by a mist of finely dispersed droplets.

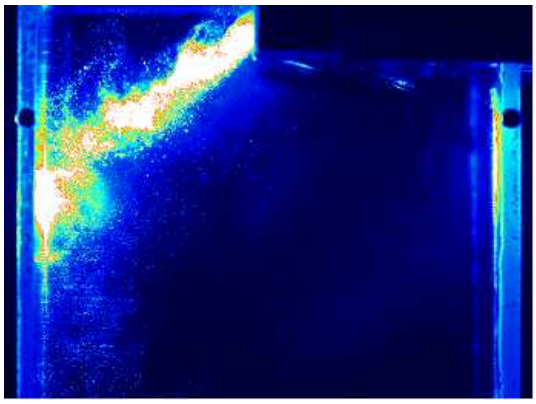

3 mm $\leq L_v \geq$ 9 mm

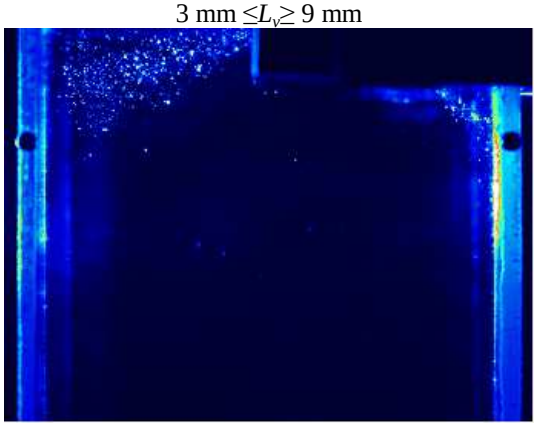

(b) 1 mm ≤L_v≥ 3 mm

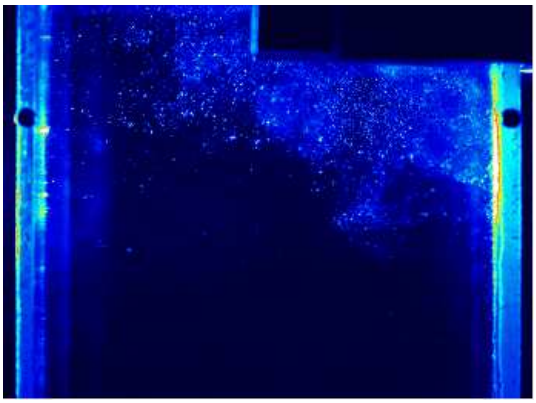

(c) 0.4 mm ≤L_v≥ 1 mm

Figure 10: Laser illumination of liquid fuel in tumble plane TP2.

The effect of the port flow velocity on the fuel spray delivery into the chamber was investigated. The arrival time of fuel in the cylinder was simplistically estimated from the penetration velocity of the leading edge of the spray determined in the quiescent study [18] divided by the distance from the injector to the valve curtain. The high-speed images were used to determine the first visual indication of fuel in the cylinder. The results showed good agreement for valve lifts of less than 3 mm in the fixed pressure drop case. For valve lifts greater than 3 mm, the arrival time of fuel was significantly reduced. A minimum of approximately 5 ms aSOI was observed at the 9 mm lift case. For valve lifts greater than 3 mm the port flow velocity accelerated the fuel spray droplets up to the free stream velocity. However, the estimated droplet Weber number, commonly used to describe the break-up of droplets in isolation, (defined as the ratio of fluid inertial forces to surface tension forces), was less than 10 in the port indicating little or no break-up. The estimated droplet Weber number for valve lifts less than 0.7 mm at the valve gap, for an air mass flow rate of 0.01 kgs^{-1} was greater than 50. This value suggested that conditions for the catastrophic break-up of fuel droplets could be expected in the valve orifice region at very low valve lifts.

3.4 Fuel droplet characteristics

The PDA study was used to determine the effect of the low valve jet flows upon the in-cylinder droplet velocities and diameters. The distribution of droplet diameters against valve lift across all of the measurement points is shown in the range plot in Fig. 11. The mean diameter plot was split into three sections labelled *1*, *2* and *3*. These sections coincided with the transitional steady flow phases previously identified. The highly dispersed region *1* consisted of droplets with an arithmetic mean diameter of 10 µm. Fig. 12 shows histogram plots for measurements taken at a valve lift of 0.4mm at the top of the cylinder, 10 mm below the gas face and 4 mm from the cylinder axis. The high data rate confirmed that the probe volume was aligned with the flow exit stream from the valve. Both the axial and radial velocity components showed a broad spread in velocity of approximately 100 ms^{-1}. The axial velocity component shows a mean velocity close to zero. A high frequency fluctuation was observed in the velocity-time series. As the probe volume was moved closer to mid-cylinder, a bimodal distribution in both the axial and radial droplet velocities was recorded.

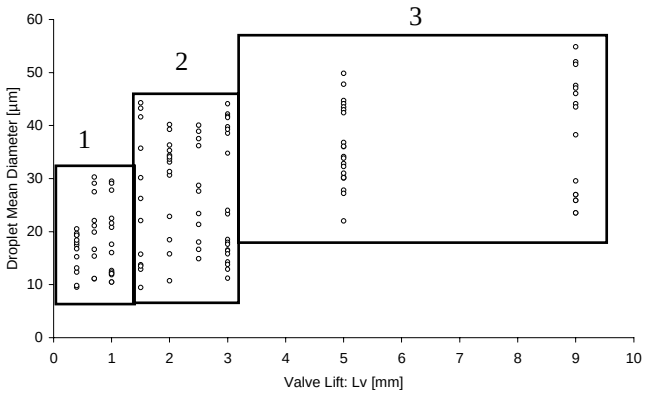

Figure 11: Range of mean droplet diameters across all measuring locations against valve lift for tumble plane TP2

A time series of the axial instantaneous droplet velocity at a valve lift of 0.4 mm and for a fixed mass flow rate of air is shown in Fig. 12. The time history of the instantaneous droplet velocity at a valve lift of 0.4 mm was divided into three phases. Phase 1 referred to the initial phase following start of injection (SOI) and related to the droplet transport time from the nozzle to the measurement location.

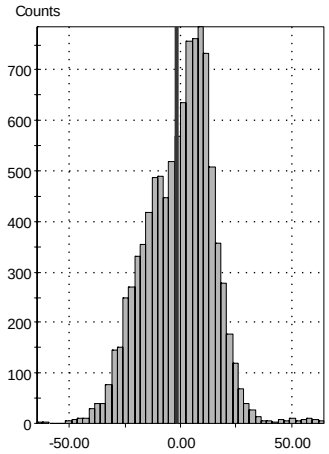

(a) Axial droplet velocity component (ms^{-1}) at 10 mm below the gas face

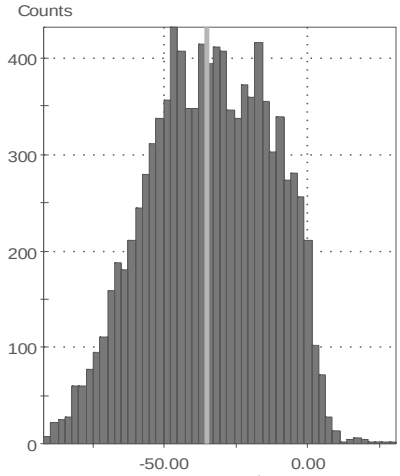

(b) Radial droplet velocity (ms^{-1}) component at 10 mm below the gas face

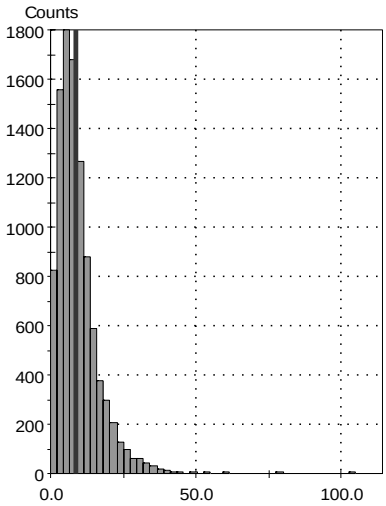

(c) Droplet diameter (μm) at 10 mm below the gas face

Figure 11: Distribution of droplet velocities and diameter for fixed flow condition of 0.01 kgs^{-1} for a valve lift of 0.4 mm in tumble plane TP2

Phase 2 was the main injection of fuel that oscillated about a zero mean axial velocity component. Phase 3 was the inter-injection phase where recorded droplets were those that had been stripped form the metal of the port and valve surfaces. They all had a positive (towards the piston) axial velocity component.

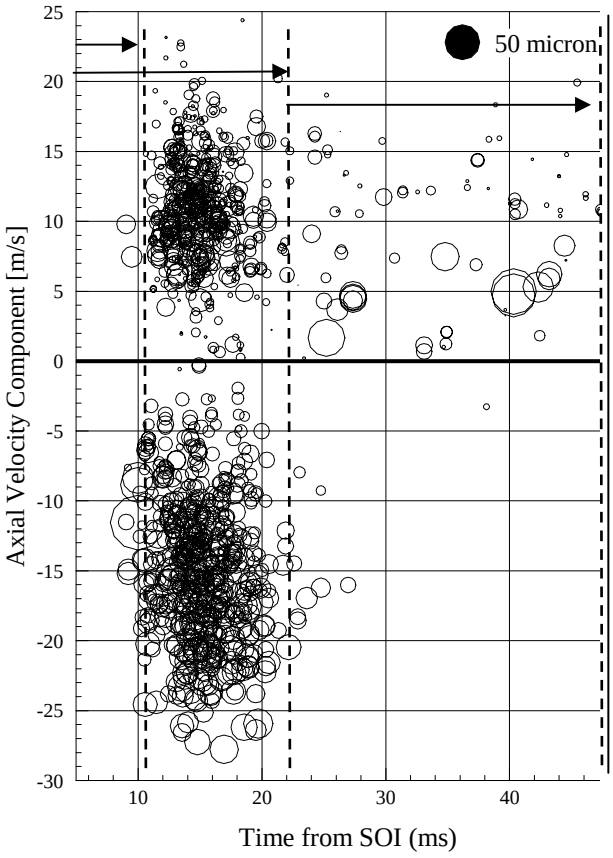

Figure 12: Time series of droplet axial velocity after SOI for fixed pressure conditions and L_v=0.4 mm

The variation in the peak, mean, steady flow fuel droplet velocity with valve lift averaged over the injection duration at a location close to the valve curtain for the fixed air mass flow rate of 0.01kgs^{-1} is shown in Fig. 13. The discharge coefficient and mean droplet diameter are also plotted for comparison.

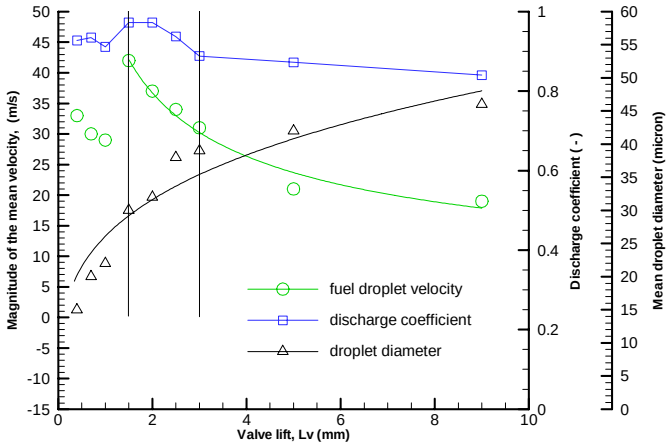

Figure 13: Variation in peak mean steady flow velocity and droplet diameter versus valve-lift for fixed flow conditions.

For valve lifts of less than 1.5mm, the discharge coefficient was slightly reduced. A significant reduction in the magnitude of the mean velocity of the fuel droplets was observed along with a reduction in droplet diameter. The best fit to the experimental data was achieved using a power function approximation using the least-squares method. The peak mean droplet velocity was approximated by $\hat{v}_{fuel} = 51L_v^{-0.5}$ for L_v greater than 1.5 mm. The mean droplet diameter was approximated by $\overline{d}_{fuel} = 26L_v^{2.8}$. For valve lifts of 1.5 to 3mm, the presence of liquid fuel in the valve gap accelerated the local air velocity and subsequently the droplet exit velocities. For valve lifts less than 1.5mm, fuel droplet break-up was dominant in the valve gap, the droplet sizes were reduced and their velocities were decreased through momentum exchange with the highly turbulent airflow.

4. CONCLUSIONS

The characteristics of the mixture preparation processes in an engine operating with a reduced peak intake valve lift have been investigated experimentally on a steady state flow rig. A BMW Valvetronic production cylinder head was modified to allow optical access to the intake port, upper cylinder and intake valve regions of the combustion chamber. The operating conditions of the steady-state flow rig have been derived from data recorded in a four-cylinder, firing engine study. A literature review has identified the key features of the mixture preparation process.

In this study, three intake valve steady flow phases have been identified; high valve lift, the first transition phase (intermediate valve lift), the second transition phase (low valve lift). At high intake valve lifts, the large intake valve orifice area has resulted in a free air jet with a mean velocity of approximately 40-50 ms^{-1} for a peak intake valve lift of 9mm and a fixed pressure drop of 40mbar, corresponding to a air mass flow rate of 0.07kg/s. The principal air flow exited over the top of the intake valves and formed a conventional, high momentum, forward tumble, mean flow pattern in the cylinder. This motion carried the fuel droplets in a similar manner over the intake valves and towards the exhaust-side chamber wall. As the air mass flow rate was reduced, the

strength of the forward tumble motion was reduced accordingly. The subsequent reduction in velocity through the valve orifice has led to an increased build up of the fuel on the intake valve surfaces. This has resulted in gravitational break-up from the intake valve surfaces. The absence of a strongly defined rotating structure has introduced flow instabilities which have been observed as variations in the axial and radial air and droplet velocity distributions. At the lowest mass flow rate condition of 0.01 kg/s, the mean droplet diameters were similar to those observed in an injector characterisation study of between 40 and 60µm [18].

As the valve lift was reduced to 3mm, a transition in the flow characteristics at the throat section was observed. This was the lowest valve lift where a forward tumble air motion was present. In the intermediate valve lift range between 3mm and 1.5mm, the measured values of the discharge coefficient were close to unity. The mean gas flow measurements have shown a twin, rotating, vortex-like structure existed within the cylinder at the 40mbar pressure drop test condition. The regions with the highest levels of turbulence intensity occurred close to the centres of the vortex-like structures. As the air mass flow rate was reduced further to 0.01kg/s, regions of high turbulence intensity highlighted the increasingly complex and multi-directional nature of the flow. A pair of high velocity jets exited either side of the intake valve. The distribution of the air velocity measurements has shown two distinctive peaks that indicated an oscillating unsteadiness close to the valve curtain. The flow of fuel droplets into the cylinder was evenly distributed around the valve periphery. The majority of droplets diameters were in the range of between 10 and 45µm. This showed a marked reduction in the diameter range in comparison with the high valve lift case. As the valve lift was further reduced from 1.5mm to 1mm, flow separation at the valve orifice increased the discharge coefficient and the tumble motion was broken down.

At the lowest valve lifts (<1mm) and air mass flow rates (for the fixed pressure drop condition of 40mbar) a weak, reverse tumble, bulk flow pattern was observed in the cylinder. The air flow measurements exhibited high frequency fluctuations. At a valve lift of 0.4mm, a narrow fuel jet was initially observed in the cylinder followed by a fuel spray mist when the air mass flow rate was increased to 0.01 kg/s, The mean air flow velocity in the valve curtain region was 45m/s. The spray aerosol comprised of droplets with diameters in the range of 2 to 30µm. The mean peak droplet velocity components were in excess of 40m/s. In this regime, the intake valve gap acted as an effective atomiser. At a location close to the intake valve, the fuel droplets exhibited a bi-modal distribution of both the axial and radial velocity components along the periphery of the main jet stream. Coincident filtering of the two velocity components (time resolved), showed that two distinct droplet size populations were measured at this location at the same time.

ACKNOWLEDGMENTS

The authors would like to thank the EPSRC equipment pool for the loan of the high-speed camera and Ricardo UK Ltd for their technical support and provision of equipment.

NOMENCLATURE

Symbol	Quantity	SI Unit
A	characteristic area	m
C_d	discharge coefficient	-
d	droplet diameter	µm
k	venturi nozzle number	-
L_v	valve lift	mm
$\dot{m}_{ac}$, $\dot{m}_{th}$	mass flow rate (measured/theoretical)	kgs^{-1}
T, p_{vent}	Temperature /absolute pressure at venturi	K / mbar
ρ_{cyl}	gas density	kgm^{-3}

REFERENCES

[1] Kramer U, Philips P. Phasing strategy for an engine with twin variable cam timing. SAE technical paper 2002-01-1101, 2002.

[2] Stone R, Kwan E. Variable valve actuation mechanisms and the potential for their application. SAE technical paper 890673, 1989.

[3] Flierl R, Klüting M. The third generation of valvetrains – new fully variable valvetrains for throttle-free load control. SAE technical paper 2002-01-1227, 2002.

[4] Hannibal W, Flierl R, Stiegler L, Meyer R. Overview of current continuously variable valve lift systems for four-stroke spark-ignition engines and the criteria for their design ratings. SAE technical paper 2004-01-1263, 2004.

[5] Mahmood Z, Chen A, Yianneskis M, Ganti G. On the structure of steady flow through dual-intake engine ports. Intl. Journal for Numerical Methods in Fluids, 1996; 23: 1085-1109.

[6] Dent J C, Chen A. An investigation of steady flow through a curved inlet port. SAE technical paper 940522, 1994.

[7] Węcłaś M, Melling A, Durst F. Combined application of surface flow visualisation and laser-Doppler anemometry to engine intake flows. Experiments in Fluids 15, 323-331 (1993).

[8] Behnia M, Milton B E. Fundamentals of fuel film formation and motion in SI engine induction systems. Energy Conversion and Management 42 (2001) 1751-1768.

[9] Brüstle C, Schwarzenthal D. Variocam plus – A highlight of the Porsche 911 turbo engine. SAE technical paper 2001-01-0245, 2001.

[10] Pietsch I, Tschöke H. Reduced intake valve lift on SI engines to improve mixture formation, fuel consumption and exhaust emissions. Ingenieurs de L´Automobile, 2002; 755: 81-85.

[11] Mischker K, Denger D. Requirements of a fully variable valvetrain and implementation using the electro-hydraulic valve control system. Proc. 24th International Vienna Engine Symposium, 2003.

[12] Takemura S, Aoyama S, Sugiyama T, Nohara T, Moteki K, Nakamura M, Hara S. A study of a continuous variable valve event and lift (VEL) system. SAE technical paper 2001-01-0243, 2001.

[13] Kreuter P, Heuser P, Reinecke-Murmann J, Erz R, Peter U, Böcker O. Variable valve actuation – switchable and continuously variable valve lifts. SAE technical paper 2003-01-0026, 2003.

[14] Milton B, Behnia M, Ellerman D. Fuel deposition and re-atomisation from fuel/air flows through engine inlet valves. Intl. Journal of Heat and Fluid Flow, 2001; 22: 350-357.

[15] Schünemann E, Münch K, Leipertz A. 1997. Interaction of Airflow and Injected Fuel Spray Inside the Intake Port of a Six Cylinder Four Valve SI Engine. SAE paper 972984.

[16] Wang Y-P, Wilkinson G.B, Drallmeier J.A. 2004. Parametric Study on the Fuel Film Breakup of a Cold Start PFI Engine; Experiments in Fluids 37, pp385-398.

[17] Costanzo V.S, Heywood J.B. 2005. Mixture Preparation Mechanisms in a Port Fuel Injected Engine; SAE paper 2005-01-2080.

[18] Begg S, Hindle M, Cowell T, Heikal M. 2007. The Effect of Intake Valve Lift on the Mixture Preparation Processes of a Port Fuel-Injected Engine. Proceedings of the 20th ECOS, Vol. 1, pp. 87-96. ISBN 88-89884-08-8. 2007.

[19] Heywood JB. Internal combustion engine fundamentals. McGraw-Hill International Editions; ISBN 0-07-100499-8, 1988.